Will anthropogenic warming increase Evapotranspiration? Examining Irrigation Water Demand Implications of Climate Change in California

P. Vahmani[1], A. D. Jones[1], and D. Li[2]

[1]Lawrence Berkeley National Laboratory, One Cyclotron Road, Berkeley, CA 94720, USA.

[2]Department of Earth and Environment, Boston University, Boston, MA, USA.

Corresponding author: Pouya Vahmani (pvahmani@lbl.gov)

Key Points:

- Increasing atmospheric temperature and vapor pressure deficit have minimal implications for evapotraspiration (ET) and irrigation water demand
- Regulation of stomata resistance by stressed vegetation offsets the expected increase in ET rates that would otherwise result from abiotic processes alone
- Anthropogenic warming of the atmosphere has minimal implications for mean relative humidity and the surface energy budget, which are critical drivers of ET

Abstract

Climate modeling studies and observations do not fully agree on the implications of anthropogenic warming for evapotranspiration (ET), a major component of the water cycle and driver of irrigation water demand. Here we use California as a testbed to assess the ET impacts of changing atmospheric conditions induced by climate change on irrigated systems. Our analysis of irrigated agricultural and urban regions shows that warmer atmospheric temperatures have minimal implications for ET rates and irrigation water demands−about one percent change per degree Celsius warming (~1 %°C^{-1}). By explicitly modeling irrigation, we control for the confounding effect of climate-driven soil moisture changes and directly estimate water demand implications. Our attribution analysis of the drivers of ET response to global anthropogenic warming shows that as the atmospheric temperature and vapor pressure deficit depart from the ideal conditions for transpiration, regulation of stomata resistance by stressed vegetation almost completely offsets the expected increase in ET rates that would otherwise result from abiotic processes alone. We further show that anthropogenic warming of the atmosphere has minimal implications for mean relative humidity (<1.7%°C^{-1}) and the surface energy budget (<0.2%°C^{-1}), which are critical drivers of ET. This study corroborates the growing evidence that plant physiological changes moderate the degree to which changes in potential ET are realized as actual ET.

1 Introduction

Irrigation is the leading source of water demand in many of the world's water-scarce regions (Brauman et al., 2016). Therefore, understanding the implications of climate change for future irrigation water demand is of critical importance as any increase in water demand could further stress already constrained water delivery systems. A vast body of literature has established a significant correlation between climatic conditions and irrigation water demand and warned that implications of climate change for precipitation, temperature, relative humidity, wind speed, etc. can lead to an increased irrigation water demand across the globe (see a review by Wang et al., 2016). However, there is little consensus on the magnitude of the predicted increases in irrigation water demand which ranges from ~3% (Ashour and Al-Najar, 2013; Anderson et al., 2008) to ~20% by the mid-century (Rodriguez et al., 2007; de Silva et al., 2007). Generally, these studies use an offline interpretation of climate model outputs and different versions of the Penman-Monteith equation and of water balance models to assess climate change impacts on irrigation demand. This approach does not allow these studies to explicitly address irrigation water demand over irrigated areas as irrigation is not represented in the majority of climate models (e.g., CMIP5). It also does not decompose dynamic representation of plant physiological components, particularly stomatal resistance and its response to climate change-induced changes in atmospheric temperature, vapor pressure deficit, or CO_2 concentrations.

The primary driver of irrigation water demand is evapotranspiration (ET). Despite its scientific and societal importance, the implication of climate change for ET and associated irrigation water demands remains uncertain, as ET is influenced by a complex array of drivers and constraints ranging from global atmospheric processes to biotic leaf-scale processes, each of which is affected by climate change to varying degrees (Katul et al., 2012). Principle among these climate-sensitive drivers is atmosphere demand in the form of vapor pressure deficit (VPD), the effect of which is modulated by wind speed and available surface radiation. ET is

also limited by available soil moisture and is regulated by plant physiology through changes in leaf stomatal conductance, which is known to respond to varying degrees to soil moisture, temperature, VPD, and atmospheric concentration of carbon dioxide (CO_2) (Katul et al., 2012).

Based on both theory and climate modeling studies, rising temperatures are expected to accelerate the global water cycle, leading to increases in both precipitation and ET (Huntington 2006; Allen and Ingram, 2002; Kunkel et al., 2013). In particular, under constant relative humidity, VPD and therefore atmospheric demand for ET are expected to track the Clausius-Clapeyron relationship, leading to approximately 6.8% increase in these quantities per degree Celsius of warming (Katul et al., 2012; Allen and Ingram, 2002; Roderick et al., 2015). Several global modeling studies project slight decreases in relative humidity over continental interiors (Fu and Feng, 2014), which would lead to even greater increases in VPD and potential ET. However, the actual precipitation and ET increases estimated by global climate models are typically much smaller than that predicted by the Clausius-Clapeyron relationship (Katul et al., 2012; Allen and Ingram, 2002; Roderick et al., 2015).

The interpretation of climate model projections as implying that "warmer is more arid" based on projected increases in potential ET is in direct contrast with paleoclimate studies and observations of 20th-century actual pan evaporation rates that imply "warmer is less arid", a dichotomy that has been termed the "global aridity paradox" (Roderick et al., 2015). Decreasing pan evaporation rates have been observed over the conterminous U.S. and Russia (Peterson et al., 1995), India, Venezuela, China, Australia, Thailand (Brutsaert, 2006), and there is evidence that global ET rates have declined during the first decade of 21st century (Wang et al., 2010; Jung et al., 2010; Miralles et al., 2014). Various studies attribute the steady decreases since the 1960s of global and regional actual ET and pan evaporation to changes in precipitation, diurnal temperature range, aerosol concentration, solar radiation, vapor pressure deficit, and wind speed (Romero-Lankao et al., 2014; Douville et al., 2013; Pan et al., 2015; Hartmann et al., 2013). Moreover, Roderick et al. (2015) demonstrate that since actual ET projected by global climate models is lower than projected potential ET, their results can be interpreted as more consistent with the observational record implying that "warmer is less arid".

One key to understanding lower projections of actual ET compared to VPD and potential ET is the role of plant stomatal conductance changes (Katul et al., 2012; Roderick et al., 2015). A recent body of literature has linked the aridity paradox to vegetation responses to rising atmospheric CO_2 concentrations (Roderick et al, 2015; Milly et al., 2017; Swann et al., 2016; Kirschbaum and McMillan 2018; Yang et al 2019), although stomatal conductance also responds to changes in soil moisture, temperature, and VPD (Katul et al., 2012). These studies support the notion that climate change has two opposing effects on ET rates: the physical implication of rising temperature and vapor pressure deficit increases ET, while stomatal closure, particularly under elevated CO_2 concentrations, acts as a restraint on ET. However, most of these efforts rely on offline interpretations of climate model outputs (e.g., CMIP5 models) in a manner that does not decompose influences from radiative, aerodynamic components, and plant physiological components.

Understanding the implications of global climate models' ET results for irrigation water demand adds one more layer of complexity. On one hand, irrigated systems are simpler than natural ecosystems in that they are intentionally maintained with adequate soil moisture for plant growth, eliminating variability in a key factor that constrains ET. However, the global climate simulations that most of the above literature is based on do not typically represent irrigation. This

makes it more difficult for the climate modeling studies to control for soil moisture availability when interpreting results, which is required to explicitly isolate the ET impacts of changing atmospheric conditions induced by climate change on irrigated systems.

Despite its drought-prone climate, California is a leading contributor to agricultural activity in the United States and home to the greatest share of the nation's population, 95% of which lives in highly irrigated urban areas (US Census Bureau, 2014) where irrigation can account for more than 50% of the municipal water consumption (Litvak et al 2017). The competing water demands for agriculture, urban areas, industry, and the environment have historically resulted in the over-allocation of watersheds in the state (California Department of Water Resources, 1998). In addition to the climate change effects on state's water supply (Hidalgo et al., 2009), it is critical to understand the implications of climate change for ET and irrigation water demands to ensure that the balance of water supply and demand levels in California can be maintained within a sustainable range (Kiparsky and Gleick, 2003; Milly et al., 2008).

In this study, we explicitly quantify the impacts of rising atmospheric temperatures on non-water limited ET and irrigation water demands in agricultural and urban areas across California (Figure 1). We use a well-established regional climate model (WRF), coupled to an urban canopy model (UCM), high-resolution remote sensing of the land surface, and realistic urban and agricultural irrigation schemes that incorporate plant physiological responses to temperature and VPD changes. We first simulate the summer irrigation season (June-Oct) for 15 historical years (2001 to 2015), then use a climate downscaling method (see Methods) that modifies the historical conditions by imposing the midcentury regional warming signal derived from two CMIP5 models (CNRM-CM5 and HadGEM2-ES) and two Representative Concentration Pathways 4.5 and 8.5 (RCP4.5 and RCP8.5), which together span the possible temperature change range for California that could be reasonably expected, bound by a 'warm' and a 'hot' scenario. Our analysis focuses primarily on irrigated urban and agricultural areas since the irrigation scheme enables us to isolate the role of atmospheric and vegetation response (as opposed to soil moisture changes) and explicitly quantify irrigation demand implications, although we include values for non-irrigated lands for comparison as appropriate.

2 Materials and Methods

2.1. WRF-UCM Configuration

We use WRF (version 3.6.1) (Skamarock et al., 2008; Skamarock and Klemp, 2008), a fully compressible, non-hydrostatic, mesoscale numerical weather prediction model. WRF is coupled with a UCM (Kusaka et al., 2001; Kusaka and Kimura, 2004) over urban areas to resolve urban canopy processes, such as shadowing, reflections, trapping of radiation, and wind profile within urban canyons, that reflect the three-dimensional nature of urban land and unique physical characteristics of built surfaces (Chen et al., 2001).

The parametrizations that represent physical processes in our WRF-UCM modeling framework include the Morrison double-moment scheme (Morrison et al., 2009) for microphysics, the Dudhia scheme (Dudhia, 1989) Rapid Radiative Transfer Model (Mlawer et al., 1997) for shortwave and longwave radiation, respectively, University of Washington (TKE) Boundary Layer Scheme (Bretherton and Park., 2009) for the planetary boundary layer, Grell–Freitas scheme (Grell and Freitas, 2014) for cumulus parameterization (used for domains d01 and d02 only), and the Eta Similarity scheme (Monin and Obukhov, 1954) for the surface layer.

We use the National Land Cover Data (NLCD) (Fry et al., 2006) for a high-resolution (30m) representation of urban and agricultural lands. We also use high-resolution (30m) NLCD impervious surface data (Wickham et al., 2006) to define impervious (or urban) fraction, independently (from land use/land cover). Urban fraction divides urban grid cells into pervious (undeveloped/vegetated) and impervious (developed) portions. We further use the National Urban Database and Access Portal Tool (Ching et al., 2009) dataset, where it is available, for a domain-specific representation of urban morphological parameters (i.e., building height, road width, etc.) in our WRF-UCM modeling framework.

Due to the importance of sea-surface temperature (SST) dynamics in shaping the regional and local climate along the California coast, we use a daily SST product (RTG_SST) produced by the National Centers for Environmental Prediction/Marine Modeling and Analysis Branch (NCEP/MMAB) in our simulations.

2.2. Modis-Based Representation Of Land Surfaces in WRF-UCM

Previous regional climate studies (Vahmani and Ban-Weiss, 2016) report that WRF-UCM performance can be improved by replacing the default climatological and tabulated representations of land surface physical characteristics with real-time high-resolution satellite-based representations of albedo, green vegetation fraction (GVF), and leaf area index (LAI). Here, we incorporate MODIS-based domain-specific real-time (2001-2015) monthly maps of green albedo, GVF, and LAI based on MODIS reflectance (MCD43A3), vegetation indices (MOD13A3), the fraction of photosynthetically active radiation (MCD15A3) products, respectively. We re-project and re-grid the MODID data to match our four WRF-UCM grids (d01, d02, d03, and d04). For more details on how remotely sensed information is interpreted for pervious and impervious surfaces in urban grid cells and comparisons between the default and improved maps of albedo, GVF, and LAI see a previous study by the authors (Vahmani and Jones, 2017).

2.3. Study Domain

We configure WRF-UCM over four two-way nested domains with horizontal resolutions of 13.5 km (domain d01), 4.5 km (domain d02), 1.5 km (domain d03), and 1.5 km (domain d04), and each with 30 vertical atmospheric levels (Fig. 1). Domain d01 covers most of the western US and parts of Mexico (Fig. 1a). Domain d02 engulfs the entire Central Valley which is a flat valley that stretches for 450 miles along with the interior of the State and holds one of the most productive agricultural regions in the US and major cities of Sacramento, Modesto, Fresno, and Bakersfield (Fig. 1b). Domains d03 and d04 cover major metropolitan areas in Northern and Southern California, respectively. Together d03 and d04 cover San Francisco Bay Area, Sacramento, Los Angeles, and San Diego (Figs. 1c and 1d).

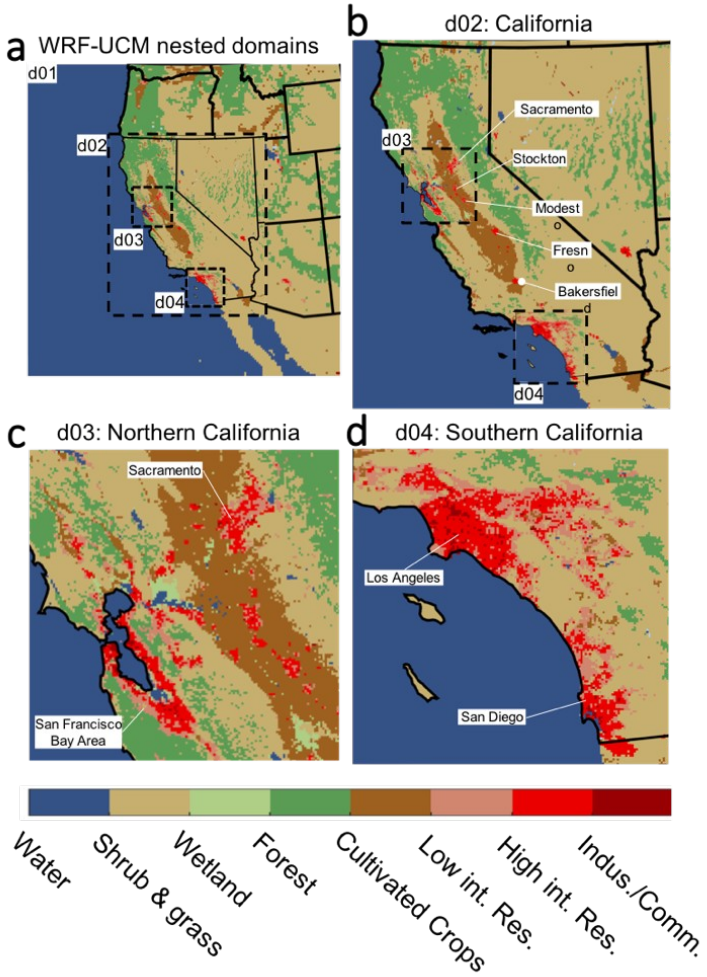

Figure 1. WRF-UCM domains: four nested domains (a) with horizontal resolutions of 13.5, 4.5, 1.5, and 1.5 km for d01, d02, d03, and d04, respectively; domain d02 (b); domain d03 (c); and domain d04 (d). Cultivated crops represent agricultural regions. Urban land classes include: low-intensity residential (Low int. res.), high-intensity residential (High int. res.), and industrial/commercial (Indus./comm.).

2.4. Simulation Design

We design three series of WRF-UCM simulations to represent the impacts of climate change on the regional and local climates and drivers of ET and irrigation water demands across urban and agricultural lands in California: one Control scenario and two mid-century climate scenarios: 'hot' and 'warm'. 'Hot' and 'warm' scenarios are driven by 1) the HadGEM2-ES GCM and RCP8.5 and 2) CNRM-CM5 GCM and RCP4.5, to represent the warmest and coolest mid-century California climate states, respectively. HadGEM2-ES and CNRM-CM5 are identified as the 'warm' and 'cool' models, respectively, by California's Fourth Climate Change Assessment (Pierce et al., 2016) from the 10 GCMs that most accurately simulate California's climate. These two models along with RCP8.5 and RCP4.5 span the possible temperature change range for California that could be reasonably expected. For each scenario, 15 WRF-UCM simulations are conducted from 20 May to 31 October 2001–2015. Considering a spin-up of 10 days, the simulations cover the growth/irrigation months of June–October over 15 years. The Control scenario represents the current climate where the boundary and initial conditions are defined based on the North American Regional Reanalysis (NARR) dataset (Mesinger et al., 2006). The climate change scenarios are designed based on a downscaling approach, described below.

Note that in reporting our results, we use the two-sided Student's t-test to evaluate the statistical significance of the changes relative to model internal variability and only report signals that are statistically significant with a 95% confidence level.

2.5. Downscaling Method (Climate Change)

Here, we follow a well-established downscaling approach (Rasmussen et al., 2011; Walton et al., 2015; Schar et al., 1996; Pall et al., 2017; Patricola et al., 2018), referred to as 'pseudo-global warming' or 'delta' method, where a climate change perturbation is introduced to the initial and boundary conditions, which are based on NARR reanalysis data in the Control or current climate scenario. The perturbations are calculated, for 1) HadGEM2-ES GCM and RCP8.5 ('hot' scenario) and 2) CNRM-CM5 GCM and RCP4.5 ('warm' scenario), as the differences in the GCMs' monthly climatology between the mid-century (2035–2064) and the historical (1993–2022) periods. The mid-century climate change signals are calculated for surface temperature, air temperature, sea surface temperature, relative humidity, wind, geopotential height, and air pressure. This delta approach reduces the potential impacts of climate models' biases on WRF-UCM results, compared to the 'direct downscaling' approach where the boundary conditions are directly derived from GCMs. This approach further allows us to control the boundary conditions that we perturbed in the climate change simulations. For this study do not change soil moisture to control for water availability and assess the implications of atmospheric states only, for ET and irrigation water demands. For the climate change scenarios, we further modified greenhouse gases (GHG) concentrations in WRF, reflecting radiative forcing of the corresponding RCP scenarios.

2.6. Irrigation Schemes

To represent irrigation and simulate the implications of climate change for irrigation water demand, we incorporate two irrigation schemes, for urban and agricultural irrigation, into the land surface model in the WRF-UCM modeling framework.

Over urban areas, we use a previously developed and validated (Vahmani and Hogue, 2014; Vahmani and Hogue, 2015) urban irrigation scheme, based on a moisture deficit function, where irrigation water is applied on a predetermined interval to the pervious portion of urban grid cells. During irrigation events, the moisture content of the topsoil layer (with a depth of 10 cm) is adjusted to the reference volumetric soil moisture threshold below which vegetation begins to stress. Urban irrigation events occur at nighttime (midnight) to avoid heavy moisture losses due to direct sun exposure. This irrigation scheme is designed to reproduce common urban irrigation behavior in that it happens at a set interval. In our simulations, urban irrigation events happen three times per week, recommended and tested by previous studies in the region (Vahmani and Hogue, 2014; Vahmani and Hogue, 2015). Note that the current irrigation scheme mimics an efficient irrigation system that avoids overirrigation or surface runoff by monitoring soil moisture to trigger and stop irrigation.

Over agricultural areas, we use a well-established (Ozdogan et al., 2010; Qian et al., 2013; Yang et al., 2017) irrigation scheme that has been implemented and validated over the California Central Valley (Yang et al., 2017). This irrigation scheme uses a green vegetation fraction (GVF) threshold and a soil moisture condition to trigger irrigation over agricultural (cultivated crops) areas, which are mapped based on a high-resolution (30 m) NLCD dataset. Irrigation is triggered when real-time MODIS-based (see above) GVF exceeds a certain GVF threshold, indicating the agricultural grid cell is in the growing season, given by:

$$GVF_{threshold} = GVF_{min} + 0.4 \times \left(GVF_{max} - GVF_{min} \right) \quad (1)$$

where GVF_{max} and GVF_{min} are MODIS-based annual maximum and minimum green vegetation fraction at an agricultural grid cell, respectively.

The soil moisture condition is defined based on a soil moisture availability factor ($SM_{available}$) that reflects soil moisture availability in the crop root-zone (Qian et al., 2013; Yang et al., 2017). $SM_{available}$ is defined as the ratio of the difference between the current root-zone soil moisture (SM) and the wilting point (SM_{WP}) and the difference between field capacity (SM_{FC}) and SM_{WP}, given by:

$$SM_{available} = \frac{SM - SM_{\wp}}{SM_{FC} - SM_{\wp}} \quad (2)$$

The soil moisture condition for irrigation is met when $SM_{available}$ falls below the threshold of 43%, recommended for California Central Valley by previous studies in the region (see Yang et al., 2017). When and where the GVF threshold and soil moisture condition are met, an irrigation event is triggered to increase the soil moisture in the root zone to the field capacity (SMFC), which is the maximum amount of moisture the unsaturated soil can hold against gravity. Similar to urban irrigation, agricultural irrigation events occur after sunset to avoid heavy moisture losses under direct sun exposure.

2.7. Attribution of Change in ET

The Penman-Monteith equation calculates ET as:

$$ET = \frac{sRn + \rho_a C_P D / r_a}{s + \gamma\left(1 + \frac{r_s}{r_a}\right)} \quad (1)$$

where Rn is available surface energy (i.e., net radiation minus ground heat flux), s is the gradient of the saturation vapor pressure with respect to temperature, ρ_a is mean air density at constant pressure, C_P is the specific heat at constant pressure, and γ is the psychrometric constant. D is the near-surface vapor pressure deficit, r_s is the bulk surface resistance, r_a is the aerodynamic resistance, and λ is the latent heat of vaporization.

According to the Penman-Monteith equation (eq. 1), five key variables are most responsible for changes in ET, that is, A, D, r_s, r_a, and s, given changes in λ are generally small. Similar to the approach adopted in Yang et al (2019), we approximate changes in ET (ΔET) as a function of its'partial differentials with respect to these five variables and changes in these variables ($\Delta R_n, \Delta D, \Delta r_s, \Delta r_a, \wedge \Delta s$) as:

$$\Delta ET \approx \frac{\partial ET}{\partial R_n}\Delta R_n + \frac{\partial ET}{\partial D}\Delta D + \frac{\partial ET}{\partial r_s}\Delta r_s + \frac{\partial ET}{\partial r_a}\Delta r_a + \frac{\partial ET}{\partial s}\Delta s \quad (2)$$

where

$$\frac{\partial ET}{\partial R_n} = \frac{s}{\lambda[s + \gamma[1 + \frac{r_s}{r_a}]]} \quad (3)$$

$$\frac{\partial ET}{\partial D} = \frac{\rho_a C_P}{\lambda r_a ¿¿} \quad (4)$$

$$\frac{\partial ET}{\partial r_s} = \frac{-\gamma[s R_n + \frac{\rho_a C_P D}{r_a}]}{\lambda r_a ¿¿¿} \quad (5)$$

$$\frac{\partial ET}{\partial r_a} = \frac{\gamma r_s[s R_n + \frac{\rho_a C_P D}{r_a}]}{\lambda r_a^{\,2} ¿¿¿} \quad (6)$$

$$\frac{\partial ET}{\partial s} = \frac{R_n}{\lambda ¿¿} \quad (7)$$

2.8. Model Validation

We validate the model performance against ground-based observations of near-surface air temperature and ET (supplementary Figs. S6 and S7). We compare simulated daily mean and maximum air temperatures to observations, based on 64 ground stations across California from the National Climatic Data Center (NCDC) network (supplementary Fig. S6). This validation analysis shows that WRF-UCM reproduces the daily temperature variations with reasonable accuracy: RMSDs of 1.1 °C and 0.4 °C for daily mean and maximum air temperatures, respectively. We future use hourly estimates of reference ET (ET0) based on ground measurements from California Irrigation Management Information System (CIMIS) stations in urban areas across California. CIMIS stations are designed to record hourly meteorological conditions over well-watered, actively growing, closely clipped grass fields. This information is then used to estimate hourly reference ET (http://www.cimis.water.ca.gov/Resources.aspx). Here, we compare WRF-UCM simulated ET, over urban landscapes (impervious or vegetated urban areas), to reference ET observations from 34 CIMIS stations (Supplementary Fig. S7). This analysis shows that the model reproduces the observed reference ETs with reasonable accuracy: RSMD of 0.6- and 0.7-mm day^{-1}, for domains d03 and d04, respectively. For both temperature and ET, we compare the observation averages from all the stations with the averages of model-simulated values from the grid-cells corresponding to the stations' locations, as it is commonly done to account for the inevitable discrepancy between the grid cell-level (1.5 km × 1.5 km) simulated values and station-based point measurements.

3 Results

Figure 2 shows that under 'hot' mid-century climate, ET rates over agricultural and urban areas and averaged over 15 years, are increased by 3.3%, which is equivalent to about one percent change per degree Celsius warming (1.4 $\%°C^{-1}$), given the average warming of 2.3°C (Supplemental Fig. S1). These results indicate an ET change rate that is much smaller than the anticipated global hydrologic cycle acceleration rate of ~6.8%$°C^{-1}$, due to the global warming temperatures, calculated based on the Clausius-Clapeyron equation (Katul et al., 2007). With small changes in ET, changes in irrigation water demand are also small: 2.6% (the equivalent of 1.1 $\%°C^{-1}$) under the 'hot' scenario. Less significant absolute changes and a similar rate change (of ~1 $\%°C^{-1}$) are found under the 'warm' scenario (Supplementary Fig. S2).

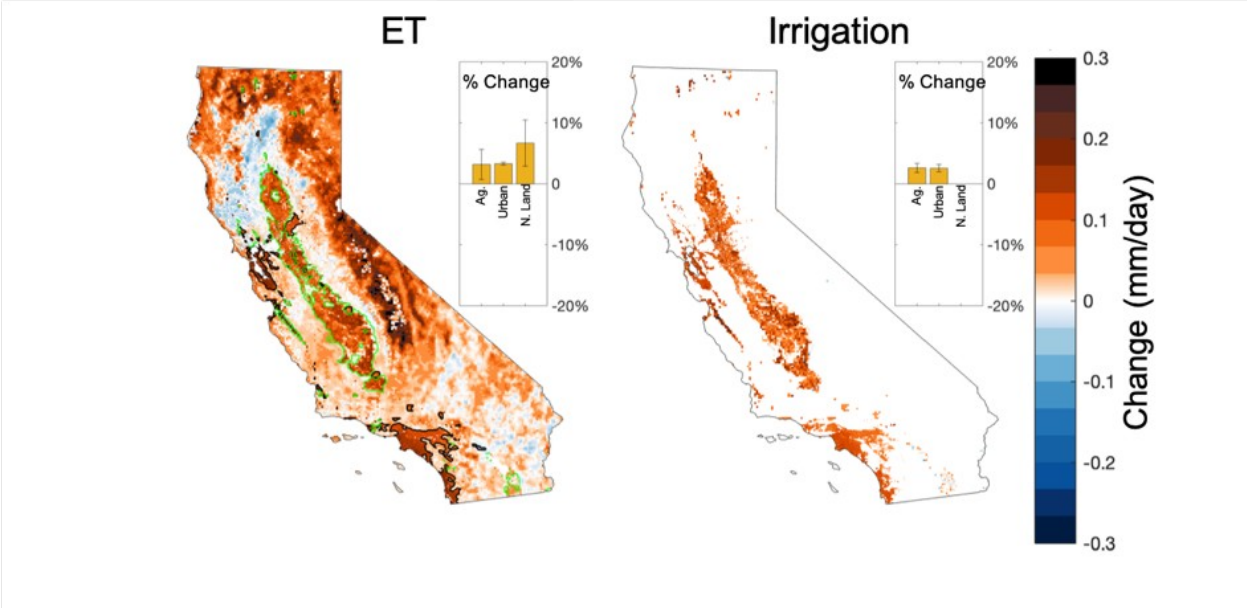

Figure 2. WRF-UCM simulated changes in ET and irrigation water demand due to Mid-century climate change under the 'hot' scenario. See Fig. S2 for the 'warm' scenario. Values are 15-year daytime averages over June-Oct. Bar plots show averages over agricultural land (Ag.), irrigated urban areas (Urban), and natural land (N. Land). Values over urban areas represent the pervious or vegetation potions only. Note that only changes that are statistically distinguishable from zero at a 95% confidence interval are included.

To understand the reasons that underpin limited ET response to warming atmospheric temperatures, we attribute mid-century ET changes to different forcing factors in the Penman-Monteith equation (see Methods) that include surface available energy (Rn: net radiation minus ground heat flux), vapor pressure deficit (D), surface resistance (rs), aerodynamic resistance (ra), and gradient of the saturation vapor pressure with respect to temperature (s). Under the 'hot' scenario, our results (Fig. 3a) show significant increases in D, rs, and s of 14%, 10%, and 12%, respectively, while changes in Rn and ra are minimal. The increases in D, rs, and s, in turn, lead to changes in ET of +7%, -6%, and +2%, adding to a total ET increases of ~+3% (Fig. 3.b). Similar pattern is found under 'warm' scenario (Supplementary Fig. S3). These results indicate that as the temperature and vapor pressure deficit in the atmosphere depart from the ideal conditions for transpiration, the regulation of stomata resistance by stressed vegetation almost completely offsets the expected increase in ET rates that would otherwise result from abiotic processes alone. These findings further show that anthropogenic warming of the atmosphere has minimal implications for mean relative humidity (<1.7% per degree C) and the surface energy budget (<0.2% per degree C), which are critical drivers of ET.

Note that the parameterization of rs in Noah LSM, incorporated in WRF, similar to many other land surface models, is based on minimum stomatal resistance (Rc_{min}), leaf area index (LAI), and four stress factors that represent the effects of solar radiation, vapor pressure deficit, air temperature, and soil moisture (Chen et al., 1996). Vegetation type and therefore Rc_{min} and LAI are constant between current and future climate scenarios in our simulations. Changes in incoming solar radiation are minimal and we control for soil moisture in our delta method (see methods) and by limiting our analysis to irrigated areas (see Supplementary Fig. S4 for change in soil moisture). Hence, the reported changes in rs are solely due to stress factors driven by air temperature and vapor pressure deficit.

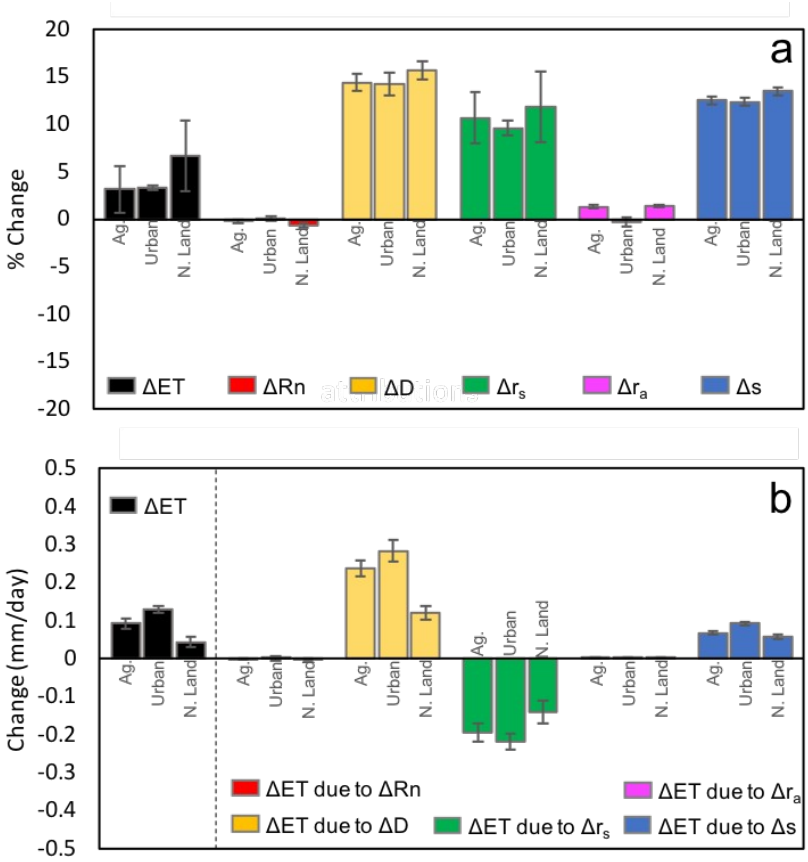

Figure 3. Climate change induced-changes in forcing factors in the Penman-Monteith equation: surface available energy (Rn), vapor pressure deficit (D), surface resistance (rs), aerodynamic resistance (ra), and gradient of the saturation vapor pressure with respect to temperature (s) (a) and attribution of changes in ET, induced by climate change, to these factors (b). The error bars illustrate the standard deviation of inter-annual fluctuations. The climate change scenario represents 'hot' mid-century. See Fig. S3 for 'warm' scenario. Values are 15-year averages over irrigated agricultural (Ag.), irrigated urban regions (Urban), and natural land (N. Land), daytime, and June-Oct. Values over urban areas are calculated for the pervious or vegetation potions. Note that only changes that are statistically distinguishable from zero at 95% confidence interval are included.

Monteith (1995) described that ET increases as D increases up to an optimal D, after which it stabilizes and eventually decreases in very dry air because of patchy closure of stomata. One interpretation of our results is that, on average, summertime vapor pressure deficit in California is at or close to the optimal value and any further increase would result in minimal ET reaction due to regulation of stomata resistance. And, continuation of drying of the atmosphere to extreme levels would result in decreasing ET rates. In the current study, we find a VPD change rate of 6.1 $\%°C^{-1}$, which is slightly lower than the rate indicated by the Clausius-Clapeyron relationship under constant relative humidity ($6.8\%°C^{-1}$). Although global climate change causes a significant change in the atmospheric temperatures (under the 'hot' scenario) and consequently in saturation vapor pressure, specific humidity also increases. Increasing specific humidity dampens increases in vapor VPD and keeps relative humidity relatively constant, especially near the coast as has been observed to date (Trenberth et al., 2007; Hartmann et al., 2013) (Fig. 4). We further find more substantial increases in VPD extremes compared to overall seasonal mean VPD (see supplemental Fig. S5) which could reach the tipping point described by Montheith (1995) and result in decreased ET rates, corroborating the findings of a recent observational study similarly showing that stomatal resistance can lead to decreases in ET during heatwave periods (Wang et al., 2019).

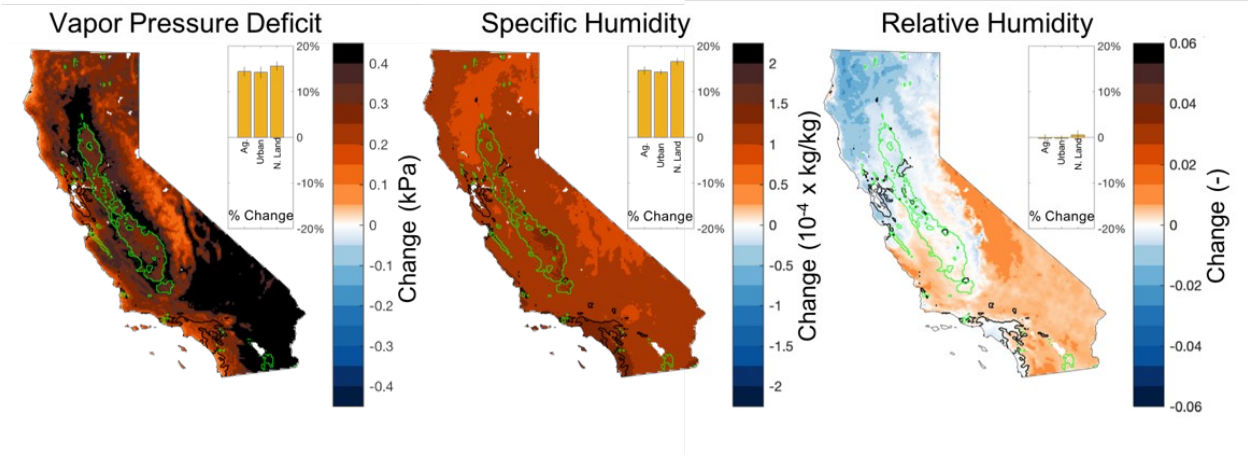

Figure 4. WRF-UCM simulated changes in vapor pressure deficit, specific humidity, and relative humidity due to Mid-century climate change under the 'hot' scenario. Values are 15-year daytime averages over June-Oct. Bar plots show averages over agricultural land (Ag.), irrigated urban areas (Urban), and natural land (N. Land). Values over urban areas represent the pervious or vegetation potions only. Note that only changes that are statistically distinguishable from zero at a 95% confidence interval are included.

Our results are broadly consistent with recent findings by Yang et al. (2019), who found that increases in stomatal resistance lead to relatively minor implications for ET rates despite a warming-induced vapor pressure deficit increase. Yang et al. (2019) attribute increased stomatal resistance to elevated CO_2 concentrations. Interestingly, we show that indirect implications of higher CO_2 concentration, higher temperatures and vapor pressure deficit, alone trigger a vegetation response that can entirely offset the D-induced changes in ET, without considering the vegetation reaction to a CO_2-enriched environment.

5 Conclusions

Here we address the 'global aridity paradox' with a case study of the implications of climate change for ET and irrigation water demand in irrigated agricultural and urban areas in California. Our results suggest that anthropogenic warming of the atmosphere and consequent elevated vapor pressure deficit have minimal implications for the future of ET rates and thereby for irrigation water demand. By controlling for water availability, we show that the warming temperatures, due to climate change under 'hot' and 'warm' scenarios, lead to ET and irrigation water demand increases of around 1 %°C^{-1}. Consistent with Roderick et al. [2015] these findings refute the common interpretation of climate modeling results as suggesting that "warmer is more arid" or that elevated temperatures amplify ET and thereby drying rates. Rather, our results indicate that warmer is neither more nor less arid.

Our attribution analysis of the drivers of ET response to global anthropogenic warming shows that as the temperature and vapor pressure deficit in the atmosphere depart from the ideal conditions for transpiration, the regulation of stomata resistance by stressed vegetation almost completely offsets the expected increase in ET rates that would otherwise result from abiotic processes alone. We further show that anthropogenic warming of the atmosphere has minimal implications for mean relative humidity (<1.7%°C^{-1}) and the surface energy budget (<0.2%°C^{-1}), which are main drivers of ET. Overall, these findings refute the notions that warming climate and resultant rising evaporative demand will lead to significant drying and indeed show that ET rates remain relatively unchanged by the warmer mid-century atmospheric temperatures.

We note that we do not consider the potential vegetation response to elevated atmospheric CO_2 concentrations, in the form of further increases in stomata resistance. We speculate that this response to higher CO_2 concentrations, in addition to the response to increasing atmospheric temperatures and vapor pressure deficit, as illustrated in this study, could lead to a tipping point where ET rates are reduced, despite higher evaporative demand in the atmosphere as has been observed [Peterson et al., 1995; Brutsaert, 2006; Wang et al., 2010b; Jung et al., 2010; Mueller et al. 2013; Miralles et al. 2014]. On the other hand, we do not explicitly consider how cropping practices might change under a warmer climate. Longer growing seasons, an extended dry season with less precipitation in the fall, and the growth of more water-intensive crops that take advantage of greater water use efficiency under elevated CO_2 conditions could all increase irrigation water demand in our study region in ways beyond the scope of the current study.

In light of the growing evidence that plant physiological changes moderate the degree to which changes in potential ET are realized as actual ET, care should be taken in interpreting studies that examine climate change implications for water demand [Wang et al., 2014; Ashour and Al-Najar, 2013; Anderson et al., 2008; Rodriguez Diaz et al., 2007; de Silva et al., 2007], drought [Diffenbaugha et al 2015; Williams et al 2015; AghaKouchak et al., 2014; Griffin and Anchukaitis, 2014; Mann and Gleick, 2015; Shukla et al., 2015; Cook et al., 2015], or wildfire [Abatzodlou and Williams, 2017; Littell et al, 2009; Littell et al., 2016; Seager et al., 2015] using temperature-based metrics such as the Palmer Drought Severity Index or related metrics based on atmospheric moisture demand or potential ET. When considering plant responses directly to temperature and VPD changes, or CO_2 change over time, actual ET may be lower than indicated by such metrics.

We note, though, that this study solely focuses on the implications of anthropogenic warming of the atmosphere for ET rates and irrigation water demand, particularly in non-water limited conditions. Climate change is still expected to impact water availability and drought and wildfire intensity and impact, for example through implications for precipitation patterns and variability, rainfall versus snow ratio, snowpack water storage, or evaporation from bare soil. Moreover, our finding that short-term extreme VPD conditions increase at a higher rate than the mean, maybe particularly important to consider in the context of wildfire management.

Acknowledgments and Data

This research was supported by the U.S. Department of Energy, O_ce of Science, as part of research in the MultiSector Dynamics, Earth and Environmental System Modeling Program. This research used resources of the National Energy Research Scientific Computing Center (NERSC), a DOE O_ce of Science User Facility supported by the O_ce of Science of the US Department of Energy under Contract No. DEAC02-05CH11231.
The WRF-UCM code, NARR, NLCD, and MODIS data, used in this study, are openly available. The deposition of the WRF-UCM data in a repository is ongoing; please contact the authors to access the data during review. We will provide a public link as soon as it is ready.

References

Abatzoglou, J. T. and A. P. Williams, Impact of anthropogenic climate change on wildfire across western US forests, 11770–11775, PNAS, October 18, 2016, vol. 113, no. 42, doi:10.1073/pnas.1607171113

AghaKouchak, A., L. Cheng, O. Mazdiyasni, and A. Farahmand (2014), Global warming and changes in risk of concurrent climate extremes: Insights from the 2014 California drought, Geophys. Res. Lett., 41, 8847–8852, doi:10.1002/2014GL062308.

Allen, M. R., and W. J. Ingram (2002), Constraints on future changes in climate and the hydrologic cycle, Nature, 419, 224–232.

Anderson J, Chung F, Anderson M, Brekke L, Easton D, Ejeta M, Peterson R and Snyder R 2008 Progress on incorporating climate change into management of California's water resources Clim. Change 87 91–108

Ashour EK, Al-Najar A (2013) The impact of climate change and soil salinity in irrigation water demand on the Gaza Strip. J Water Clim Chang 4(2):118–130

Brauman, K. A., Richter, B. D., Postel, S., Malsy, M. & Florke, M. Water depletion: an improved metric for incorporating seasonal and dry-year water scarcity into water risk assessments. Elem. Sci. Anth. 4, 000083 (2016).

Bretherton CS and Park S 2009 A new moist turbulence parameterization in the community atmosphere model J. Climate 22 3422–48

Brutsaert, W. B. (2006), Indications of increasing land surface evaporation during the second half of the 20th century, Geophys. Res. Lett., 33, L20403, doi:10.1029/2006GL027532.

California Department of Water Resources, 1998. California Water Plan. Updated Bulletin 160-98. California Department of Water Resources, Sacramento, CA.

469 Chen F et al 2011 The integrated WRF/urban modeling system: development, evaluation, and
470 applications to urban environmental problems Int. J. Climatol. 31 273288

471 Chen Fei, Kenneth Mitchell, John Schaake, Yongkang Xue, Hua-Lu Pan, Victor Koren, Qing Yun
472 Duan, Michael Ek, and Alan Betts, Modeling of land surface evaporation by four
473 schemes and comparison with FIFE observations, JOURNAL OF GEOPHYSICAL
474 RESEARCH, VOL. 101, NO. D3, PAGES 7251-7268, MARCH 20, 1996

475 Ching J et al 2009 National urban database and access portal tool Bull. Am. Meteorol. Soc. 90
476 1157–68

477 Cook, B. I., T. R. Ault, and J. E. Smerdon (2015), Unprecedented 21st century drought risk in the
478 American Southwest and Central Plains, Sci. Adv., 1(1), e1400082,
479 doi:10.1126/sciadv.1400082.

480 de Silva CS,Weatherhead EK, Knox JW, Rodriguez-Diaz JA (2007) Predicting the impacts of
481 climate change—a case study of paddy irrigation water requirements in Sri Lanka. Agr
482 Water Manag 93(1):19–29

483 Diffenbaugha, N. S., D. L. Swaina, and D. Toumaa, Anthropogenic warming has increased
484 drought risk in California, PNAS, March 31, 2015, vol. 112, no. 13, 3931–3936,
485 doi:10.1073/pnas.1422385112

486 Douville, H., A. Ribes, B. Decharme, R. Alkama, and J. Sheffield (2013), Anthropogenic
487 influence on multidecadal changes in reconstructed global evapotranspiration, Nat. Clim.
488 Change, 3, 59–62.

489 Dudhia J 1989 Numerical study of convection observed during the winter monsoon experiment
490 using a mesoscale two dimensional model J. Atmos. Sci. 46 3077–107

491 Fry J A, Xian G, Jin S, Dewitz JA, Homer CG, Yang L, Barnes CA, Herold N Dand Wickham
492 JD2012Completion of the 2006 National Land Cover Database update for the
493 Conterminous United States Photogramm. Eng. Remote Sens. 77 858–64

494 Fu, Q., and S. Feng, 2014: Responses of terrestrial aridity to global warming. J. Geophys. Res.
495 Atmos., 119, 7863–7875, doi:10.1002/2014JD021608.

496 Grell G A and Freitas S R 2014 A scale and aerosol aware stochastic convective parameterization
497 for weather and air quality modeling Atmos. Chem. Phys. 14 5233–50

498 Hartmann, D. L., et al. (2013), Observations: Atmosphere and surface, in Climate Change 2013:
499 The Physical Science Basis. Contribution of Working Group I to the Fifth Assessment
500 Report of the Intergovernmental Panel on Climate Change, edited by T. F. Stocker et al.,
501 pp. 159–254, Cambridge Univ. Press, Cambridge, U. K.,
502 doi:10.1017/CBO9781107415324.008.

503 Hidalgo, H.G., Das, T., Dettinger, M.D., Cayan, D.R., Pierce, D.W., Barnett, T.P., Bala, G.,
504 Mirin, A., Wood, A.W., Bonfils, C., Santer, B.D., Nozawa, T., 2009. Detection and
505 attribution of streamflow timing changes to climate change in the western United States.
506 Journal of Climate 22, 3838–3855.

507 Huntington, T. G. (2006), Evidence for intensification of the global water cycle: Review and
508 synthesis, J. Hydrol., 319, 83–95.

509 Jung, M., M. Reichstein, P. Ciais, S. Seneviratne, J. Sheffield, et al. (2010), Recent decline in
510 global land evapotranspiration trend due to limited moisture supply, Nature, 467, 951–
511 954.

512 Katul, G. G., R. Oren, S. Manzoni, C. Higgins, and M. B. Parlange (2012), Evapotranspiration: A
513 process driving mass transport and energy exchange in the soil-plant-atmosphere-climate
514 system, Rev. Geophys., 50, RG3002, doi:10.1029/2011RG000366.

515 Kiparsky, M., Gleick, P.H., 2003. Climate Change and California Water Resources: A Survey and
516 Summary of the Literature. California Climate Change Center, Report no. CEC-500-04-
517 073.

518 Kirschbaum, M. U. F. & A. M. S. McMillan, Warming and Elevated CO2 Have Opposing
519 Influences on Transpiration. Which is more Important?, Current Forestry Reports (2018)
520 4:51–71, doi:10.1007/s40725-018-0073-8

521 Kunkel, K. E., T. R. Karl, D. R. Easterling, K. Redmond, J. Young, X. Yin, and P. Hennon
522 (2013), Probable maximum precipitation and climate change, Geophys. Res. Lett., 40,
523 1402–1408, doi:10.1002/grl.50334.

524 Kusaka H and Kimura F 2004 Coupling a single-layer urban canopy model with a simple
525 atmospheric model: impact on urban heat island simulation for an idealized case J.
526 Meteorol. Soc. Japan 82 67–80

527 Kusaka H, Kondo H, Kikegawa Y and Kimura F 2001 A simple singlelayer urban canopy model
528 for atmospheric models: comparison with multi-layer and slab models Bound. Layer
529 Meteorol. 101 329–58

530 Littell JS, Peterson DL, Riley KL, Liu Y, Luce CH (2016) A review of the relationships between
531 drought and forest fire in the United States. Glob Change Biol 22(7): 2353–2369.

532 Litvak E, McCarthy HR, Pataki DE. 2017. A method for estimating transpiration of irrigated
533 urban trees in California. Landscape and Urban Planning 158: 48–61.

534 Mesinger F et al 2006 North American regional reanalysis Bull. Am. Meteorol. Soc. 87 343 60

535 Milly, P. C. D. & Dunne, K. A. A hydrologic drying bias in water−resource impact analyses of
536 anthropogenic climate change. J. Am. Water Resour. Assoc. 53, 822–838 (2017).

537 Milly, P.C.D., Betancourt, J., Falkenmark, M., Hirsch, R.M., Kundzewicz, Z.W., Lettenmaier,
538 D.P., Stouffer, R.J., 2008. Stationarity is dead: whither water management? Science 319,
539 573–574.

540 Miralles, D., et al. (2014), El Niño-La Niña cycle and recent trends in continental evaporation,
541 Nat. Clim. Change, 4, 122–126.

542 Mlawer E J, Taubman S J, Brown PD, IaconoMJ and Clough SA 1997 Radiative transfer for
543 inhomogeneous atmospheres: RRTM, a validated correlated-k model for the longwave J.
544 Geophys. Res. 102 16663–82

545 Monin A S and Obukhov AM 1954 Basic laws of turbulent mixing in the surface layer of the
546 atmosphere Contrib. Geophys. Inst. Acad. Sci. USSR 151 163–87 (in Russian)

547 Monteith, J. L. (1995), A reinterpretation of stomatal responses to humidity, Plant Cell Environ.,
548 18, 357–364, doi:10.1111/j.1365-3040.1995.tb00371.x.

549 Morrison H, Thompson Gand Tatarskii V 2009 Impact of cloud microphysics on the
550 development of trailing stratiform precipitation in a simulated squall line: comparison of
551 one– and two–moment schemes Mon. Weather Rev. 137 991–1007

552 Ozdogan, M., M. Rodell, H. K. Beaudoing, and D. L. Toll, 2010: Simulating the effects of
553 irrigation over the United States in a land surface model based on satellite-derived
554 agricultural data. J. Hydrometeor., 11, 171–184, doi:10.1175/2009JHM1116.1.

555 Pall P, Patricola CM, Wehner MF, StoneDA, Paciorek Cand CollinsWD2017 Diagnosing
556 conditional anthropogenic contributions to heavy colorado rainfall in September 2013
557 Weather Clim. Extremes 17 1–6

558 Pan, S., H. Tian, S. Dangal, Q. Yang, J. Yang, C. Lu, B. Tao, W. Ren, and Z. Ouyang (2015),
559 Responses of global terrestrial evapotranspiration to climate change and increasing
560 atmospheric CO2 in the 21st century, Earth's Future, 3, 15–35,
561 doi:10.1002/2014EF000263.

562 Patricola CM and Wehner MF 2018 Anthropogenic influences on major tropical cyclone events
563 Nature 563 339–46

564 Peterson, T. C., et al. (1995), Evaporation losing its strength, Nature, 377, 687–688,
565 doi:10.1038/377687b0.

566 Pierce DW, Cayan DR and Dehann L 2016 Creating Climate projections to support the 4th
567 California Climate Assessment (La Jolla, CA: Division of Climate, Atmospheric
568 Sciences, and Physical Oceanography, Scripps Institution of Oceanography)

569 Qian, Y., M. Huang, B. Yang, and L. K. Berg, 2013: A modeling study of irrigation effects on
570 surface fluxes and land–air–cloud interactions in the southern Great Plains. J.
571 Hydrometeor., 14,700–721, doi:10.1175/JHM-D-12-0134.1.

572 Rasmussen R et al 2011 High-resolution coupled climate runoff simulations of seasonal snowfall
573 over Colorado: a process study of current and warmer climate J. Climate 24 3015–48

574 Roderick, M. L., P. Greve, and G. D. Farquhar (2015), On the assessment of aridity with changes
575 in atmospheric CO2, Water Resour. Res., 51, 5450–5463, doi:10.1002/2015WR017031.

576 Rodriguez Diaz JA, Weatherhead EK, Knox JW(2007) Climate change impacts on irrigation
577 water requirements in the Guadalquivir River basin in Spain. Reg Environ Chang 7:149–
578 159

579 Romero-Lankao, P., J.B. Smith, D.J. Davidson, N.S. Diffenbaugh, P.L. Kinney, P. Kirshen, P.
580 Kovacs, and L. Villers Ruiz, 2014: North America. In: Climate Change 2014: Impacts,
581 Adaptation, and Vulnerability. Part B: Regional Aspects. Contribution of Working Group
582 II to the Fifth Assessment Report of the Intergovernmental Panel on Climate Change
583 [Barros, V.R., C.B. Field, D.J. Dokken, M.D. Mastrandrea, K.J. Mach, T.E. Bilir, M.
584 Chatterjee, K.L. Ebi, Y.O. Estrada, R.C. Genova, B. Girma, E.S. Kissel, A.N. Levy, S.
585 MacCracken, P.R. Mastrandrea, and L.L. White (eds.)]. Cambridge University Press,
586 Cambridge, United Kingdom and New York, NY, USA, pp. 1439-1498.

587 Schär C, Frei C, Lüthi D and DaviesHC1996 Surrogate climate-change scenarios for regional
588 climate models Geophys. Res. Lett. 23 669–72

589 Seager R, et al. (2015) Climatology, variability, and trends in the U.S. vapor pressure deficit, an
590 important fire-related meteorological quantity. J Appl Meteorol Climatol 54(6):1121–
591 1141.

592 Shukla, S., M. Safeeq, A. AghaKouchak, K. Guan, and C. Funk (2015), Temperature impacts on
593 the water year 2014 drought in California, Geophys. Res. Lett., 42, 4384–4393,
594 doi:10.1002/2015GL063666.

595 Skamarock W. C. and Klemp J B 2008 A time-split nonhydrostatic atmospheric model for
596 research andNWP applications J. Comput. Phys. 227 3465–85

597 Skamarock W. C., Klemp J B, Dudhia J, GillDO, BarkerDM, DudaMG, Huang X-Y, WangWand
598 Powers JG 2008 A description of the advanced researchWRFVersion 3 NCAR Technical
599 NoteNCAR/TN-475+STR National Center for Atmospheric Research
600 (https://doi.org/10.5065/D68S4MVH)

601 Swann, A. L. S., Hoffman, F. M., Koven, C. D. & Randerson, J. T. Plant responses to increasing
602 CO2 reduce estimates of climate impacts on drought severity. Proc. Natl Acad. Sci. USA
603 113, 10019–10024 (2016).

604 Trenberth KE, Jones PD, Ambenje P, Bojariu R, Easterling D, Klein Tank A, et al. Surface and
605 atmospheric climate change. In: Solomon S, Qin D,ManningM, Chen Z, Marquis M,
606 Averyt KB, Tignor M, Miller HL, editors. Climate change 2007: the physical science
607 basis. Contribution of Working Group I to the Fourth Assessment Report of the
608 Intergovernmental Panel on Climate Change. Cambridge: Cambridge University Press;
609 2007. p. 235–336.

610 US Census Bureau (2014) State and County QuickFacts. Available at https://www.census.
611 gov/quickfacts.

612 Vahmani P and Ban-Weiss GA 2016 Impact of remotely sensed albedo and vegetation fraction on
613 simulation of urban climate in WRF-urban canopy model: a case study of the urban heat
614 island in Los Angeles J. Geophys. Res. Atmos. 121 1511–31

615 Vahmani P and Jones AD 2017 Water conservation benefits of urban heat mitigation Nat.
616 Commun. 8 1072

617 Vahmani, P. & Hogue, T. Incorporating an urban irrigation module into the Noah Land surface
618 model coupled with an urban canopy model. J. Hydrometeorol. 15, 1440–1456 (2014).

619 Vahmani, P. & Hogue, T. S. Urban irrigation effects on WRF-UCM summertime forecast skill
620 over the Los Angeles metropolitan area. J. Geophys. Res. Atmos. 120, 9869–9881 (2015).

621 Walton DB, Sun F, Hall A and Capps S 2015 A hybrid dynamical-statistical downscaling
622 technique: I. Development and validation of the technique J. Clim. 28 4597–617

623 Wang X, Zhang J-Y, Shahid S, Guan E-H, Wu Y-X, Gao J and He R-M 2016 Adaptation to
624 climate change impacts on water demand Mitig. Adapt. Strateg. Glob. Change 21 81–99

625 Wang, K., R. Dickinson, M. Wild, and S. Liang (2010), Evidence for decadal variation in global
626 terrestrial evapotranspiration between 1982 and 2002: 2. Results, J. Geophys. Res., 115,
627 D20113, doi:10.1029/2010JD013847.

628 Wang, P., D. Li, W.L. Liao, A. J. Rigden, W. Wang, (2019). Contrasting Evaporative Responses
629 of Ecosystems to Heatwaves Traced to the Opposing Roles of Vapor Pressure Deficit and
630 Surface Resistance Water Resour. Res.

631 Wickham JD, Stehman SV, Gass L, Dewitz J, Fry JA and Wade TG2013 Accuracy assessment
632 ofNLCD2006 land cover and impervious surface Remote Sens. Environ. 130 294–304

633 Williams, A. P., R. Seager, J. T. Abatzoglou, B. I. Cook, J. E. Smerdon, and E. R. Cook (2015),
634 Contribution of anthropogenic warming to California drought during 2012–2014,
635 Geophys. Res. Lett., 42, 6819–6828, doi:10.1002/2015GL064924.

636 Yang Y., M. L. Roderick , S. Zhang, T. R. McVicar and R. J. Donohue, Hydrologic implications
637 of vegetation response to elevated CO2 in climate projections, NATURE CLIMATE
638 CHANGE, VOL 9, JANUARY 2019, 44–48, doi:10.1038/s41558-018-0361-0

639 Yang Z, Dominguez F, Zeng X, Hu H, Gupta H, Yang B (2017) Impact of irrigation over the
640 California Central Valley on regional climate. J Hydrometeorol.
641 https://doi.org/10.1175/JHM-D-16-0158.1